Green Chemistry

PAPER

View Article Online
View Journal | View Issue

Cite this: *Green Chem.*, 2024, **26**, 8256

Wood-inspired dual-scale directional channel cellulose bioreactors with high mass transfer efficiency for continuous flow catalytic green conversion†

En-Jiang Liu,‡ Yu-Shi Shen,‡ Mei-Yan Ling, Chen-Xi He, Xing Zhou, Jun Wang, Shuai You, Wei-Guo Zhao, Xiao-Hui Yao and Dong-Yang Zhang *

Received 15th November 2023,
Accepted 8th January 2024

DOI: 10.1039/d3gc04421a

rsc.li/greenchem

In recent years, microfluidic bioreactors have become important in chemical production; however, the production cost is high, and it becomes difficult to balance scale, efficiency, and cost. Therefore, a low-cost, efficient, high-delivery-capacity, green-fluid reactor is urgently required. Herein, a cellulose bioreactor with dual-scale directional channels and a porous inner wall is reported for the continuous catalytic conversion of polydatin into resveratrol. The dual-scale directional channel structure endows the reactor with high mass transfer speed and large transport capacity, resulting in fast fluid diffusion rate and more severe "disturbance" inside the reactor. It accelerates the mass transfer state of the whole reaction and further improves the catalytic performance compared to the uniform channel reactor. The reactor can achieve a high conversion rate of 98.58% of resveratrol within 2 h and exhibits excellent stability, owing to which it has broad application prospects in catalytic reactions, and helps derive a new approach for constructing fluid catalysis bioreactors.

Introduction

Fluid biocatalysis has considerably improved the efficiency of chemical reactions owing to its high-efficiency and strong selectivity. It has become one of the green technologies in sustainable chemistry and plays an important role in daily life.[1–3] Although fluid catalytic devices can provide highly ordered flow regimes to accelerate catalytic reactions, their applications are still limited by throughput, fluid pressure drop, and channel blockage.[4] In recent years, continuous catalytic immobilized enzyme reactors with directional channels have attracted considerable interest, because they generate low pressure and enable rapid flow.[5–7] In this type of reactor, the substrate in the channel quickly interacts with the catalyst to achieve efficient reaction, and several processes, such as subsequent centrifugal separation, are avoided, considerably reducing the process energy consumption and cost.[8,9] In addition, owing to the relatively uniform channel, industrial problems caused by pressure drop have been considerably improved.[10] However, most directional channel reactors still need to be realized *via* etching, resulting in high cost and a limited number of etched channels, and can only achieve small-scale production, which cannot effectively expand the production scale and balance efficiency, cost, and scale.[11] Therefore, there is an urgent need to design a high-efficiency fluid catalytic bioreactor with high-throughput and low-pressure drop that can be prepared easily and quickly.

The abundant directional channels in natural wood provide it with efficient nutrient transport capacity and the ability to achieve a good balance between throughput and pressure drop, making it one of the excellent choices for reactor materials.[12] Moreover, owing to ray cells and pits in the cell wall, the fluid in the channel can interact with adjacent channels to achieve intermittent changes in the direction of fluid flow and accelerate the radial transport of substances.[13,14] It results in favorable conditions for the catalytic reaction. In our previous study, a cellulose bioreactor with directional channels, *e.g.*, xylem, was successfully constructed *via* freeze casting.[15] The constructed reactor exhibits excellent bidirectional mass transport (longitudinal and radial) and more adequate fluid interaction compared to wood, which achieves efficient product conversion. The results of this study indicate that fluid interaction ("disturbance") occurs mostly in places with large differences in internal channels and is considerably

College of Biotechnology and Sericultural Research Institute, Jiangsu University of Science and Technology, Zhenjiang, 212100, PR China.
E-mail: dongyang_zhang1987@126.com; Fax: +86 511 85616777;
Tel: +86 511 85616777

†Electronic supplementary information (ESI) available. See DOI: https://doi.org/10.1039/d3gc04421a

‡Co-first authors.

correlated to the size of internal channels in the reactor. Therefore, the "disturbance" needs to be further strengthened by adjusting the internal channel size to improve the catalytic efficiency of the reactor.

Herein, a construction strategy is proposed for a dual-scale hierarchical directional channel microfluidic reactor with high throughput, performance, and stability is proposed. By adjusting the substrate material to regulate the growth of ice crystals during freeze casting, two different sizes of ice templates coexist in the same material, thereby constructing dual-scale directional channels. The changes in the motion state of the fluid in the reactor and the impact of different structures on catalytic performance are explored. It is proven that the dual-scale directional microreactor exhibits a higher substrate conversion rate and higher stability than the uniform channel bioreactor. This dual-scale reactor can maintain low-flow pressure while aggravating the disturbance of the internal fluid, thereby increasing the probability of enzyme contacting the substrate and improving the mass transfer efficiency. The reactor can be easily manufactured, inexpensive, and stable activity, which makes it widely usable in industrial flow catalytic reactions.

Materials and methods

Materials and reagents

Cellulose (cotton linter pulp) was purchased from Hubei Chemical Fiber Group Co., Ltd, China. Urea, sodium hydroxide (NaOH), epichlorohydrin (EPI), ethanol, *p*-nitrophenol glucoside (*p*-NPG), citric acid, and disodium hydrogen phosphate were purchased from Sinopharm Chemical Reagent Co., Ltd, China. These chemicals and solvents were of analytical grade and used without further purification.

Preparation of a cellulose reactor

Cotton was dissolved at a low temperature in a 100 mL sodium hydroxide/urea/pure water system. After further dissolution *via* two to three times homogenization at 8000 rpm, 2 mL of EPI was added to crosslink for 2 h, and a uniform 2 wt% cellulose solution was obtained *via* centrifugation using liquid nitrogen as a coolant and a three-layer ring-shaped metal rod as a frozen annular substrate. The cellulose solution was added to the mold, the mold was placed on the top device, and under low-temperature unidirectional conduction, the solvent was frozen in the solution to form an ice crystal template.[16] The frozen cellulose block was freeze-dried for 48 h, and the ice template was removed to obtain oriented microchannels with different diameters. Fig. S1a† shows the image of the cellulose reactor with a white color.

Enzyme immobilization

The ammonia solution was pumped into the cellulose sample using a single-channel pump at 50 °C to fully react with the epoxy group introduced before. Then, the β-glucosidase solution was pumped into the materials to complete the covalent fixation of the enzyme using 2.5% glutaraldehyde solution as a crosslinking agent.[17] As shown in Fig. S1b,† an apparent color change was clearly observed after enzyme immobilization.

Characterization

The morphology of the transverse/longitudinal interface of the lyophilized cellulose was observed *via* field emission scanning electron microscopy (SEM) (QUANTA 250 FEG, Thermo Fisher, America). X-ray diffraction (XRD) (D8 Advance, Bruker, Germany) was used to analyze changes in the crystal structure of cellulose samples before and after treatment. X-ray photoelectron spectroscopy (XPS) (AXIS, Shimadzu, Japan) was used to analyze the surface elements of cellulose samples before and after enzyme fixation. The chemical structure of each cellulose sample was determined and analyzed *via* Fourier transform infrared (FT-IR) spectroscopy (NicoLet iS5, Thermo Fisher, USA).

Analysis of the activity of free and immobilized enzymes

Different concentrations of *p*-NPG solutions were mixed, 1 M Na_2CO_3 was added, and absorbance values were measured at a wavelength of 410 nm. The standard curve equation was plotted using the concentration of *p*-NPG solution as the abscissa and the absorbance value as the ordinate. *p*-NPG was dissolved in the PBS buffer (pH 5) at 5 mM. For free enzymes, 200 and 100 μL of enzyme solution were mixed, and the reaction was performed at 50 °C for 10 min. The reaction was immediately stopped by adding 1-M Na_2CO_3, and the color was displayed. Absorbance values were measured at 410 nm. The enzyme activity was measured based on the standard curve.[18]

Effects of pH, temperature, and reaction time on free and immobilized enzyme activity

Using the resveratrol side as a substrate, the catalytic activities of free enzyme and immobilized enzyme were measured at different pH values (pH 4–8) and temperatures (20 °C–60 °C). The polydatin and resveratrol concentrations in the reaction solution were determined *via* high performance liquid chromatography, and the conversion rate was calculated. The transformation was analyzed under different conditions.

Continuous catalytic reaction in a reactor

The polydatin solution was injected into the cellulose immobilized enzyme reactor through the continuous fluid catalytic device (Fig. S1c†), and the catalytic reaction was repeated for 3 h. After the reaction, 1 mL of solution and pass it through 0.22 μM filter membrane filtration, followed by HPLC analysis and detection. The polydatin and resveratrol concentrations before and after hydrolysis were calculated and compared. After the completion of the reaction, the residual solution was washed with deionized water, the aforementioned steps were repeated, the reuse rate of the reactor was calculated, and the stability of the reactor was investigated.[19]

Statistical analysis

The experimental results of the three repeated tests are expressed in mean ± standard deviation.

Results and discussion

Construction strategy for the dual-scale microfluidic reactor

During freeze casting, the speed, direction, and temperature of ice-crystal growth during the solidification stage are controllable.[20,21] The growth of ice crystals can be controlled by adjusting the temperature gradient to provide ice templates of different scales to obtain channels of different sizes. Herein, a ring-shaped freezing substrate was designed. Metals with different thermal conductivities were combined to realize the coexistence of two temperature gradients on the same substrate, allowing ice crystals to grow under the two gradients, providing a dual-scale ice crystal template to construct dual-scale directional channel structures (Scheme 1a). The growth of the ice template was controlled by adjusting the metal substrate, and the corresponding channel structure was adjusted to form additional disturbances to strengthen mass transfer (Scheme 1b).

Construction and morphology analysis of a single-medium cellulose reactor

Four kinds of metals (copper, aluminum, iron, and stainless steel) with different thermal conductivity values were selected to prepare cellulose materials with different channel structures, and the internal structure of the materials was observed (Table S1†). All the materials exhibited directional channels and porous inner wall structures (Fig. 1). The stainless-steel substrate exhibited the largest channel diameter, followed by iron, aluminum, and copper. The channel size and thermal conductivity of the metal substrate exhibited a negative correlation trend. The larger the temperature gradient in the freeze casting stage, the faster the growth of ice crystals and the smaller the diameter of the obtained channels.[22] This result was consistent with the SEM results. It was further verified using pore size analysis (Fig. S2†). The feasibility of channel aperture control by adjusting the substrate was demonstrated, which makes it possible to construct dual-scale directional channel structures.

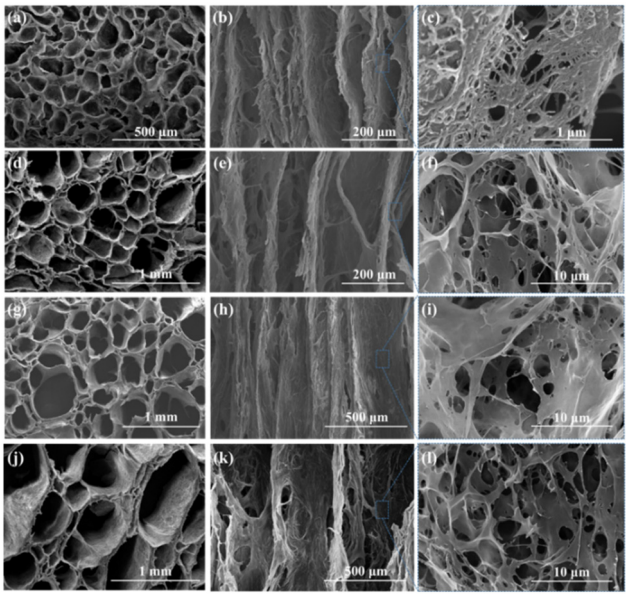

Fig. 1 Scanning electron microscopy (SEM) morphologies of cellulose reactors prepared with different substrates: (a–c) copper; (d–f) aluminum; (g–i) iron; (j–l) stainless steel.

Construction and morphology analysis of a dual-scale cellulose reactor

Copper (highest thermal conductivity) was used for the low-temperature zone, and the metal substrate in the sub-low-temperature zone was changed to construct a ring-shaped substrate for freeze casting to explore the changes in the internal structure of cellulose reactors. Different reactors exhibited directional channels and porous inner wall structures, and the cross-section SEM images illustrated the successful construction of dual-scale directional channels (Fig. 2). The copper–stainless steel combination (CE-STs) exhibited the largest middle channel diameter. With an increase in the thermal conductivity of the substrate, the channel diameter in the sublow temperature zone decreased and the channel wall became thinner (Fig. 2 and S3†). In CE-ST, the sizes of the middle channel ranged from 650 to 750 μm (accounting for approximately 38% of the total volume), copper–iron (CE-I) ranged from 450 to 500 μm (36%), and copper–aluminum (CE-A) ranged from 400 to 460 μm (26%). The channel size of the corresponding reactor obtained using a single-metal substrate was similar. In addition, the channel size of the low-temperature zone was similar to that of the copper-based cellulose reactor (CE-C). The feasibility of using the ring substrate to construct dual-scale directional channels and the successful construction of dual-scale reactors were verified.

The dual-scale channel was further verified by the transmission of the optical path (Fig. S4†). The dual-scale and

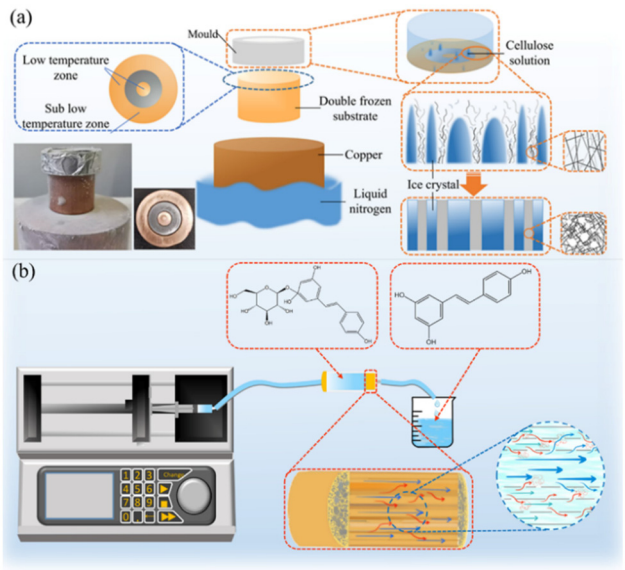

Scheme 1 (a) Use of dual-scale ice crystal template constructing dual-scale directional channel structures; (b) construction of a dual-scale cellulose reactor and the formation of additional disturbances.

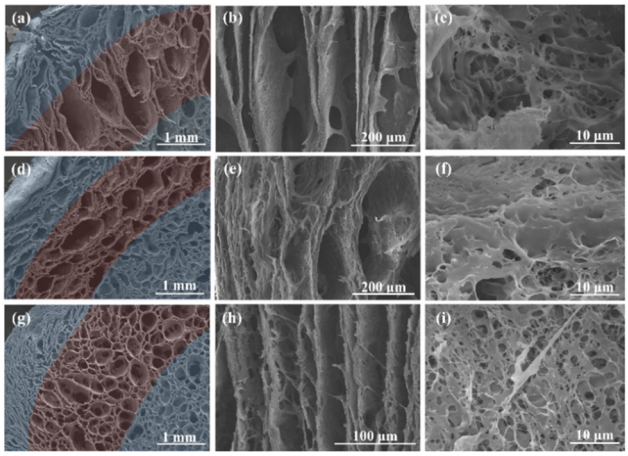

Fig. 2 SEM morphologies of cellulose reactors prepared with different substrates: (a–c) copper–stainless steel; (d–f) copper–iron; (g–i) copper–aluminum.

uniform reactors were used to irradiate the laser at different positions, and the spot status of the bottom plate was observed (Fig. S4a†). Only when irradiating the middle channel (large channel) of the dual-scale directional channel reactor (Fig. S4a1†), the bottom plate could receive light spots, whereas at other positions with a small channel diameter, the light path transmission was hindered; the bottom plate received fuzzy halo (Fig. S4a2–4†). It verified the successful construction of the dual-scale channel structure. In addition, both reactors exhibited considerable radial light transfer under the light from the vertical channel direction, attributed to the abundant pores on the inner wall of the reactors (Fig. S4b,† the *X*-axis direction). The dual-scale channel structure reactor possessed a wider and brighter light spot range, which exhibited better permeability than that of the uniform microchannel structure.

To study the changes in the chemical composition before and after treatment, the linters and cellulose materials were analyzed using XRD. The peak positions after treatment shifted from 14.8°, 16.5°, and 22.7° to 12.1°, 20.1°, and 22.1°, respectively, transitioning from typical cellulose I to cellulose II (Fig. S5†); moreover, crystallinity decreased (Table S2†). This is consistent with the report that natural cellulose can be regenerated from cellulose I to cellulose II after alkali treatment.[23] The bulk density and porosity of the material were determined and analyzed (Table 1), which changed slightly with decreasing in thermal conductivity.

Table 1 Physical parameters of different materials

	Diameter (μm)				
	Small	Large	Ratio	Bulk density (g cm^{-3})	Porosity (%)
CE-C	110	110	1/1	0.064	95.99
CE-A	98	410	1/4	0.067	95.78
CE-I	100	470	1/5	0.063	96.08
CE-STs	105	680	1/6	0.074	95.40

Enzyme immobilization

To achieve stable enzyme immobilization, β-glucosidase was covalently immobilized on different cellulose materials (CE-C, CE-A, CE-I, and CE-STs) to prepare bioreactors (the covalent immobilization principle is shown in Fig. 3a). The reactors were named CER1/1, CER1/4, CER-1/5, and CER1/6 according to the ratio of large and small directional channel diameters. CER-1/6 was selected as a representative to study changes in the chemical structure of the material. The FT-IR spectra of the free enzyme and cellulose reactor before and after enzyme immobilization are shown in Fig. 3b. The spectra of the free enzyme indicated the corresponding vibrational absorption peak of the protein molecular skeleton.[24] The peaks at 2936 and 1654 cm^{-1} are attributed to the C–H stretching vibration of the protein alkyl group and the C=O stretching vibration of the acetylamino group, respectively. The C–H angle-change

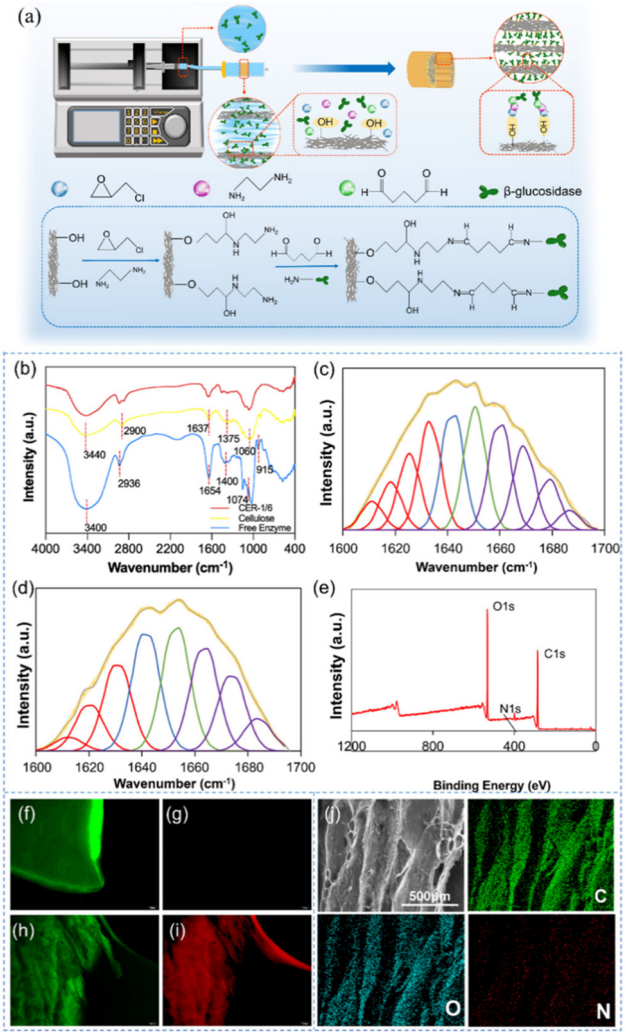

Fig. 3 (a) Immobilized enzyme process; (b) FT-IR spectra of different materials; infrared deconvolution maps of amide: (c) free enzyme; (d) CER-1/6; (e) X-ray photoelectron spectroscopy (XPS) spectrum analysis of CER-1/6; (f–g) CE-STs in green and red fluorescence; (h–i) CER-1/6 in green and red fluorescence; (j) EDS spectra of CER-1/6.

vibration value of the peptide bond of the protein molecule was 1400 cm^{-1}, and the characteristic peaks of pyranose ring ether bond and D-glucose pyranose were observed at 1074 and 915 cm^{-1}, respectively. For cellulose, absorption peaks were observed at 3440, 2900, 1637, 1375, and 1060 cm^{-1}, which were attributed to the stretching vibration of –OH, C–H, C=O, C–H, and C–O in cellulose, respectively.[25] The absorption peaks of cellulose and enzyme protein molecules can be observed in CER-1/6 at the same time, confirming the successful immobilization of the enzyme protein.

As chemical treatment would affect the secondary structure of protein, the amide absorption peak in the spectra of the free enzyme and CER-1/6 was deconvoluted (Fig. 3c and d).[26] After chemical covalent fixation, the concentrations of α-helix and β-sheet in the enzyme protein decreased by approximately 10%, whereas those of β-turns and random coil increased (Table S3†), indicating that the hydrogen bonds in the folded chains were broken, the structure of the enzyme protein became loose, and the internal hydrophobic groups might be exposed. It is reported that chemical covalent crosslinking may cause the partial unfolding of enzyme proteins, which is consistent with the aforementioned results.

XPS was used to further explore the changes in the groups of the materials (Fig. 3e and S6†). In the C1s spectrum of CE, the peaks at 284.60, 286.49, and 287.96 eV belong to C–C, C–O, and O–C–O/C=O, respectively. The peaks at 532.15 and 532.94 eV in the O1s spectrum correspond to C–OH and C–O–C, respectively. Similarly, these peaks appeared in CER-1/6 (Fig. S7 and Table S4†). The content of the C–C group in the XPS spectrum of CER-1/6 considerably increased, and in addition to the two peaks of C 1s and O 1s, a new N peak appeared, confirming the successful covalent immobilization of enzyme after crosslinking with glutaraldehyde.

For further verification, fluorescence staining was performed on the materials before and after immobilization (Fig. 3f–i). Enzyme protein and CER-1/6 were stained with rhodamine B (red) and fluorescein isothiocyanate (green), respectively. The unimmobilized enzyme cellulose material emitted light under green fluorescence (Fig. 3f and g), whereas the immobilized material exhibited a complete cellulose skeleton within red and green excitation wavelengths; the contours were consistent with each other (Fig. 3h–i), confirming the uniform immobilization of the enzyme on the reactor. Moreover, the distribution of N elements along the channel was observed in the energy-dispersive X-ray spectroscopy (EDS) spectrum, which further verified the success of enzyme immobilization (Fig. 3j).

Catalytic activity of the bioreactor

As the catalytic activity of the enzyme after covalent immobilization is affected by its own conformation and catalytic environment,[27] the catalytic conditions of the enzyme were optimized. Considering CER-1/6 as the representative reactor, the catalytic conversion rates of free and immobilized enzyme materials were measured at pH 6–8 and 30 °C–80 °C to determine the optimal conversion conditions (Fig. 4a and b).

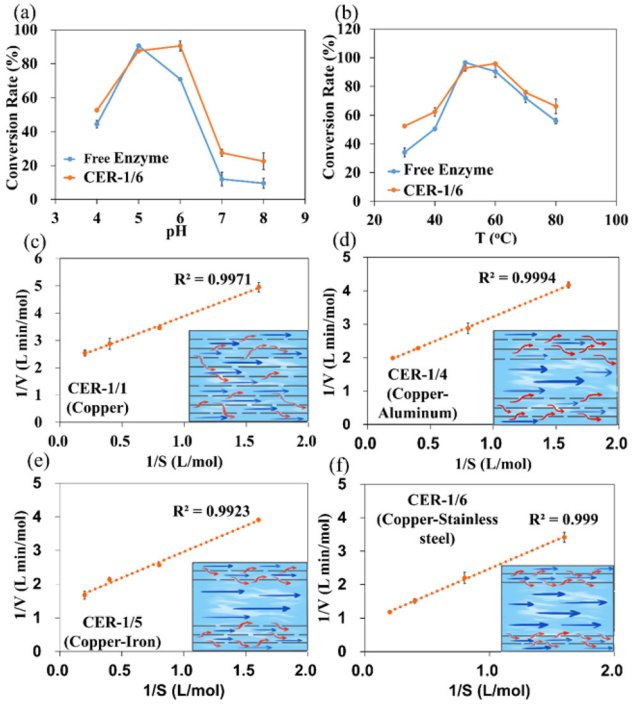

Fig. 4 Conversion rates of free enzyme and CER-1/6 under different conditions: (a) pH; (b) T. Kinetic curves of bioreactor with different materials: (c) CER-1/1; (d) CER-1/4; (e) CER-1/5; (f) CER-1/6.

After immobilization, enzymes exhibit better stability than free enzymes at different pH values and temperature and can still maintain good activity at high temperatures (60 °C–80 °C) under alkaline conditions. The maximum conversion rates of the immobilized enzyme materials were 92.56% and 95.85% at a pH value of 6 and 60 °C, whereas those of free enzymes were 90.64% and 96.63% at a pH value of 5 and 50 °C. CER-1/6 exhibited more advantages with regard to the conversion rate of resveratrol compared to free enzymes, as it might be related to the internal channel structure of the immobilized material. The constructed directional channel, porous inner wall structure, and hydrophilic characteristics provide a better catalytic microenvironment for enzyme catalysis (Fig. S8†).

The kinetic parameters of free enzymes and reactors with different structures (different combinations of large and small directional channel) were further measured and calculated based on the Lineweaver Burk diagram (Fig. 4c–f, S9,† and Table 2). The K_m value of free enzyme was 0.643 mM, and V_{max} was 0.589 mmol min^{-1}. After covalently immobilizing, K_m increased. The lower the apparent K_m value, the higher the affinity of the enzyme to the substrate, and the faster the maximum reaction rate. Owing to changes in the enzyme structure and diffusion limitations within the material, the affinity of the enzyme to the substrate often decreased, thereby decreasing the maximum reaction rate.[28,29] The V_{max} value of the dual-scale reactors (CER-1/4, CER-1/5, and CER-1/6) are higher than that of the free enzyme and uniform channel reactors (CER-1/1), indicating the good catalytic potential of the

Table 2 K_m and V_{max} values of different materials

	K_m [mM]	V_{max} [mmol min^{-1}]
Free enzyme	0.643	0.589
CER-1/1	0.792	0.460
CER-1/4	0.945	0.603
CER-1/5	1.102	0.710
CER-1/6	1.831	1.144

dual-scale channel structure reactor. In addition, with an increase in the ratio of large and small channels, the V_{max} value of the reactor increased. CER-1/6 exhibited the highest reaction rate (1.144 mmol min^{-1}), which was nearly twice that of free enzyme. The ratio of large and small channels inside the reactor may considerably impact the mass transfer efficiency.

Study on the catalytic performance of the bioreactor

In the continuous flow catalytic process, flow rate is one of the important factors affecting reaction efficiency. Therefore, the conversion rates of four reactors with different structures were measured at different flow rates (Fig. 5a). With an increase in the flow rate, the conversion rate of each reactor gradually decreased. The conversion rate of CER-1/6 decreased from 94.65% to 80.27%, and those of CER-1/5 and CER-1/4 decreased by 22.97% and 38.60%, respectively; the conversion rate of CER-1/1 decreased by approximately 50%, which was about 3.5 times that of CER-1/6. The reactor with the dual-scale channel structure exhibited better adaptability at different flow rates, with CER-STs, indicating the best stability. Changes in the flow rate alter the residence time of the fluid in the channel and the fluid morphology on the channel surface, thereby affecting the catalytic results. When the flow rate is low, the fluid stays in the channel for a longer time and is more likely to collide with the fluids in adjacent channels through small pores on the wall, increasing the collision frequency of enzyme and substrate; thus, the reaction is more sufficient. In addition, the three dual-scale reactors exhibited better adaptability than the uniform channel reactor (CER-1/1) at different flow rates, and the conversion rates were all higher than that of CER-1/1, which confirmed the good catalytic potential of the dual-scale reactor. CER-1/6 exhibited the best stability; the larger the ratio of the size of the channels, the more efficient the mass transfer inside the reactor.

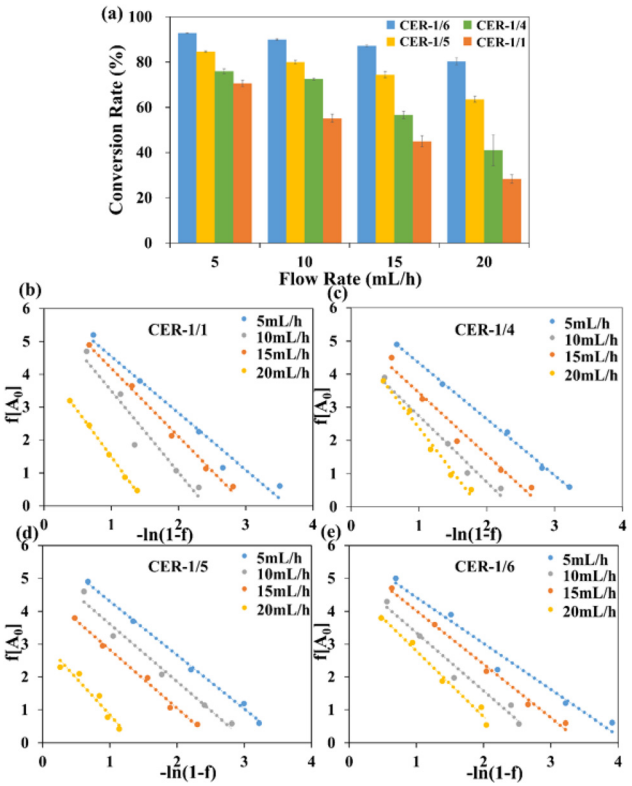

Fig. 5 (a) Effect of the flow rate on the enzyme reaction efficiency; hydrodynamic kinetics curves of bioreactors with different materials: (b) CER-1/1; (c) CER-1/4; (d) CER-1/5; (e) CER-1/6.

The hydrodynamic parameters of CERs with different structures were further analyzed and explained based on the Lilly–Hornby model. The results are shown in Fig. 5b–e. After linear fitting calculation, the values of K'_m at different flow rates are listed in Table 3. Different K'_m values indicate that the apparent kinetics of the reactor are influenced by mass transfer effects. Under the same reactor, as the flow rate increased, K'_m increased. The smallest K'_m was observed at a flow rate of 5 mL h^{-1}, indicating that the interaction between the enzyme and substrate was more effective and the catalytic efficiency was higher at this time. This result is consistent with the conversion result. The dual-scale reactors exhibited smaller K'_m values than the uniform channel reactor (CER-1/1) at different flow rates, among which CER-1/6 exhibited the smallest value, indicating that the dual-scale directional channel structure can provide better affinity between catalyst and substrate and is more conducive to catalytic reactions. This conclusion is consistent with the aforementioned conversion results It is proved that the greater the difference in channel diameter, the better the diffusion of the substrate in the reactor and the higher mass transfer efficiency.

Analysis of the improvement of the catalytic efficiency of the reactor

To further investigate the reasons for the efficiency improvement of dual-scale directional channel reactors, models of uniform nonporous channels (Fig. 6a), uniform porous channels (Fig. 6b), and dual-scale directional channel structures (Fig. 6c) were constructed using COMSOL Multiphysics based

Table 3 Hydrodynamic parameters at different flow rates (K'_m)

	5 mL h^{-1}	10 mL h^{-1}	15 mL h^{-1}	20 mL h^{-1}
CER-1/1	1.730	2.083	2.480	2.787
CER-1/4	1.692	1.878	1.990	2.667
CER-1/5	1.640	1.756	1.787	2.244
CER-1/6	1.403	1.630	1.771	2.008

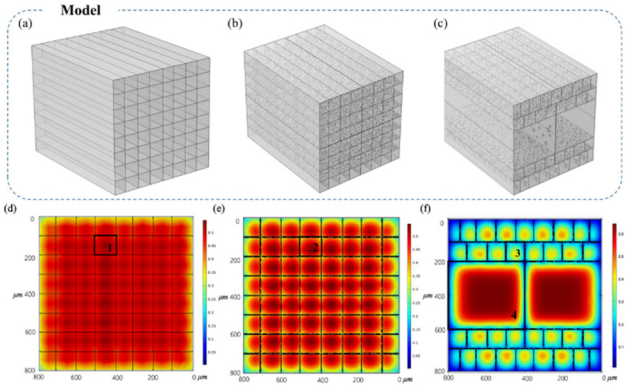

Fig. 6 Models of reactors with different structures: (a) uniform nonporous channel; (b) uniform porous channel; (c) dual-scale channel; cloud diagram of substrate concentration changes: (d) uniform nonporous channel; (e) uniform porous channel; (f) dual-scale channel.

on SEM and pore size statistical analysis results for substrate concentration field simulation. The effect of different channel structures on the catalytic reaction was studied according to the substrate concentration. The profile reaction inside the reactor after 10 min was selected, and the change in concentration is shown in Fig. 6d–f. The concentration of the substrate within the channel represented the degree of reaction, where a lower substrate concentration indicated a higher degree of completion of the reaction inside the channel. Compared with the nonporous structure (concentration of substrate in the center of the channel: 0.54 mol m^{-3}), the porous inner wall considerably improved the overall catalytic efficiency of the reactor. The reactions in the inner channels were sufficient, and the center concentrations of the channels were 0.51 (uniform porous channel) and 0.41 mol m^{-3} (dual-scale channel). This is because the fluid entered the adjacent channel from the pores on the wall while moving. Owing to the differences in flow direction and velocity, the fluid entering the channel collides with the fluid in the adjacent channels, forming "disturbance" to accelerate mass transfer and improve the reaction rate,[30,31] which verify the advantages of the porous inner wall structure. In addition, four locations of the profiles in the three models illustrated in Fig. 6d–f (zones 1, 2, 3, and 4) and S8.† Although the large channel (zone 4, Fig. S10b†) in the dual-scale directional channel structure exhibits insufficient reactions within the channel because of the longer diffusion path, the central concentration is still not considerably different from that in the uniform channel material (approximately 0.1 mol m^{-3}). Moreover, the proportion of large channels in the reactor is only 25%, and the main reaction efficiency of the reactor is still partially dominated by small channels, while the reaction efficiency in the small channels (zone 3, Fig. S10a†) is considerably higher than that in the uniform channel model (zones 1 and 2, Fig. S10a†). The substrate concentration distribution curve implies that the substrate concentration in the uniform channel is 1.3 times that in the dual-scale directional channel (the higher the remaining substrate concentration, the slower the reaction), which indicates the excellent reaction efficiency of the dual-scale directional structure. It was confirmed that the addition of large channels could accelerate the reaction in small channels while maintaining a certain reaction rate, thus further improving the overall catalytic efficiency. The presence of porous inner walls and dual-scale channels has considerably improved the catalytic efficiency of the reactor, and the larger the proportion of large and small channels, the more significant the improvement is. This conclusion is consistent with the kinetic study.

The residence time distribution (RTD) in the reactor has an important influence on the catalytic performance of the reactor.[32–36] In the CSTR, the RTD directly affects the contact degree of the catalyst and the substrate, and the higher RTD facilitates the further improvement of the catalytic performance of the reactor.[32,33] In this study, the fluid flow state in uniform porous and dual-scale channels was studied (Fig. 7). The simulation results show that the interaction between adjacent channels of fluids in the small channel of the dual-scale structure is more obvious than that in the uniform porous one, and there are more "disturbance" phenomena (Fig. 7a–d). Moreover, as the ratio of large and small channels increases, the fluid interaction in small channels increases, and the collision further reduces the fluid velocity, with a wider and deeper range of blue areas (Fig. 7b–d). Compared to the uniform channel, the flow velocity in the small channel of the dual-scale structure is nearly 1/10 of that. As the channel ratio increases, the flow velocity of the fluid in the large channel is further reduced due to the "disturbance" caused by the interaction between fluids, from 0.15 m s^{-1} (CER-1/4) to 0.13 m s^{-1} (CER-1/6). Similar to the CSTR, the slower flow velocity leads to a higher RTD, and the higher RTD of the substrates and catalysts contact makes the reaction more complete.[32,33] The decrease in the flow rate prolongs the residence time of the substrate in the reactor, increases the contact probability of the enzyme and the substrate, and thus accelerates the reaction process. Therefore, the simulation results further confirm that the addition of large channels can effectively enhance mass transfer inside the bioreactor, improve the RTD of both large and small channels, and the larger the channel ratio, the

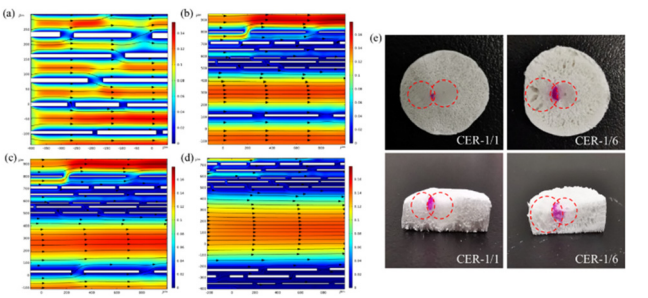

Fig. 7 Velocity field simulation diagram of fluid flow: (a) CE-Copper; (b) CE-Aluminum; (c) CE-Iron; (d) CE-Stainless steel. (e) Liquid diffusion of CER-1/1 and CER-1/6.

more intense the effect. The simulation results agree with the conversion rate results of different materials and the concentration simulation results, indicating the advantages of the dual-scale structure in enzyme catalysis.

The liquid diffusion experiment was used to further study the motion state of the fluid inside the reactor. Two syringes containing phenolphthalein and sodium hydroxide solutions were fixed to the syringe pump to build a liquid diffusion device (Fig. S11†). A dual-scale reactor, a uniform channel reactor, and delignified wood were fixed to the syringe to inject the phenolphthalein and sodium hydroxide solutions into the material simultaneously. As a phenolphthalein solution appears red when it reacts with alkaline sodium hydroxide, the mixing of the two solutions can be verified by the red area to determine the mixing mass transfer of fluid in the material. Owing to the small dense internal channels of the delignified wood, the solution could not enter the channels at high flow rates, and the liquid seeped out from the injection surface, indicating two independent circular imprints on the surface of the material, and longitudinal transmission was not observed (Fig. S12†). Compared to wood, cellulose reactors exhibited better longitudinal and radial diffusion (Fig. 7e), both reactors have red areas, confirming the intersection of the two solutions during the motion process. This result agreed with the fluid motion simulation results, verifying that the fluid can generate "disturbance" with adjacent channels through pores on the wall, providing sufficient material transport for the reactor. The diffusion areas of the two liquids in CER-1/1 were similar due to their uniform channels, while CER-1/6 exhibited a wider area in the larger channel section. The large channel can provide larger transmission capacity and accelerate liquid diffusion. In addition, compared to CER-1/1, the red part of CER-1/6 exhibited a larger area and deeper depth in the longitudinal direction, which indicates that in a dual-scale structure, fluids can frequently communicate between large and small channels, and "microdisturbances" inside the channels are more abundant. This result agreed with the simulation results, verifying that the dual-scale structure exhibits stronger material transport capabilities compared to the uniform structure.

In industrial production, the internal pressure of the reactor play an important factor in measuring its stability. Excessive internal pressure drop may cause reactor damage and reduce stability. Therefore, the pressure field of different structures in the flow catalytic system was simulated and measured (Fig. S13 and S14†). Compared with the uniform channel, the dual-scale channel exhibited a smaller pressure gradient in the pressure field, and the larger the channel ratio, the further the pressure gradient decreased, which was also confirmed by the actual measurement. When the same reactors were combined, the actual pressure measured by CE-STs was 0.20 kPa, which was 3/5 of that of CE-C and much smaller than that of wood with directional channel structure (3.90 kPa). It is reported that the existence of macroscopic pores can increase channel transport capacity and reduce internal pressure.[37] This conclusion is consistent with the aforementioned results, further providing assurance for the stability of the reactor.

Fluid catalytic performance of the dual-scale cellulose bioreactor

Resveratrol is a natural phenolic compound with good physiological activity.[38] Related studies extracted resveratrol from mulberry (*Morus alba*) with a wide ecological distribution.[39–41] However, most resveratrol still exists in nature in the form of glycosides, and direct extraction of resveratrol from plants is not only high cost but also low yield.[42,43] Moreover, the biological potency of glycosides is far lower than its aglycones.[44,45] Therefore, it is of high importance to transform polydatin into resveratrol through a continuous fluid catalytic system (Fig. 8a). Dual-scale cellulose bioreactors (CE-1/6) were used to catalyze the conversion of polydatin under the optimal reaction conditions to determine the conversion efficiency, reusability and storage stability of the reactors. The results are illustrated in Fig. 8.

Before the reaction, the concentrations of polydatin and resveratrol were 171.50 ± 2.173 and 1.08 ± 1.416 μg mL^{-1}, respectively. After 2 h of biotransformation, the concentration of polydatin decreased to 2.42 ± 0.925 μg mL^{-1}, and the concentration of resveratrol increased to 69.64 ± 3.013 μg mL^{-1} (Fig. 8b and S15†). The conversion rate can reach 98.58%. Compared to CER-1/1 and delignified wood (wood-d) (uniform channel), the dual-scale reactor exhibited more advantages, with a conversion rate 1.2 times higher than that of uniform channel reactor (Fig. 8c). This confirms the considerable improvement in catalytic efficiency facilitated by the dual-scale channel structure. The conversion rate was considerably higher than those of previous reports as well (Table 4).[46–49] Compared to cellulose microspheres and other column reac-

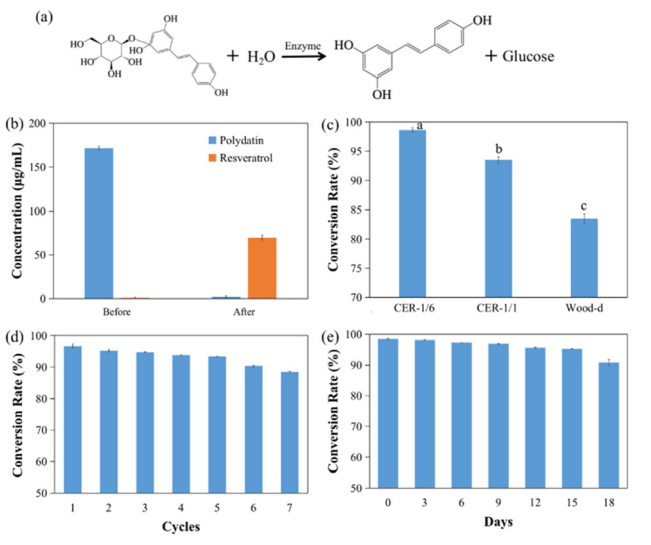

Fig. 8 (a) Transformation of polydatin and resveratrol; (b) concentration changes in polydatin and resveratrol before and after transformation; (c) conversion rates of CER-1/6, CER-1/1, and Wood-d; (d) recycling degree of CER-1/6; (e) storage stability of CER-1/6.

Table 4 Comparison of different methods of conversion, from polydatin into resveratrol

Methods	Times (h)	Conversion rate (%)
Magnetically fixed Bacillus natto[46]	48	98.60
Immobilized *Aspergillus* Niger and yeast fermentation[47]	46	96.70
Cellulose microspheres immobilized β-glucosidase[48]	8	93.06
Bioreactor with high-speed counter-current chromatography[49]	25	90.82
CER-1/6	2	98.58

tors, CBR-1/6 exhibited higher conversion rates and shorter reaction times. In addition, the preparation and operation costs of this bioreactor were more cost-effective and efficient, with lower energy consumption, making it suitable for reactions of different scales. Although other immobilized microbial reactors can achieve similar conversion rates, the required time is approximately 16 times than that of CER-1/6.[46,47] Moreover, due to the growth and metabolism of microorganisms, these reactors produce impurities, leading to the requirement of subsequent processes, such as separation and purification, which increase energy consumption and cost. In contrast, CER-1/6 not only uses its dual-scale structure to achieve efficient and stable transformation but also simplifies the production processes of upstream and downstream industries at low cost, thereby indicating its excellent application potential. Related studies have also prepared directional channel reactors similar to this study to convert polydatin into resveratrol (Table S5†).[15,18] Compared to other reactors, the CER-1/6 prepared in this study has the lowest Km value (1.8 mM), indicating that the enzyme in CER-1/6 has the highest affinity for substrates, resulting in a maximum reaction rate of 1.1 mmol min^{-1}. In addition, CER-1/6 can achieve a conversion rate of up to 98.58% in just 2 hours. The reaction time of other reactors was 3 hours and 4 hours respectively, and the conversion rate is only 0.86 higher than CER-1/6. In addition, the space–time-yield (STY) of free enzyme and CER-1/6 were also calculated. As shown in Fig. S16,† the STY of the free enzyme converting polydatin to resveratrol was 6.74 mg g^{-1} h^{-1}, and the STY of CER-1/6 was 17.13 mg g^{-1} h^{-1}. The STY of CER-1/6 is more than 2.5 times of the free enzyme, showing good catalytic performance CER-1/6.

The reusability and storage stability of the reactor were also measured, respectively (Fig. 8d and e). After seven cycles of usage, the reactor still achieved a conversion rate of >90%, and no material collapse was evident, indicating relatively stable conversion performance. After 18 days of storage, the conversion efficiency of the reactor decreased by approximately 10%. These results not only confirmed the excellent application potential of the dual-scale cellulose bioreactor, but also further promote the application of this green natural polymerization of cellulose in the field of new functional materials.[50–53]

Conclusions

In this study, an efficient and stable fluid catalytic bioreactor with a dual-scale directional channel structure was developed. The coexistence of two size of channels in the reactor was achieved by controlling the growth of ice crystals during casting by changing the combination of metal substrates. In this structure, the combination of large and small channels not only improved the transport speed and capacity of reactors but also ensured the transport capacity under low energy consumption. In addition, the mass transfer efficiency of the reactor was further improved due to the abundant pores in the wall of the reactor. Based on these characteristics, the reactor achieved a conversion rate of 98.58% for polydatin within 2 h. Even at a high flow rate of 20 mL h^{-1}, the internal flow pressure in the reactor is 0.20 kPa. It was confirmed that dual-scale reactors exhibit more sufficient internal micro disturbances under fluid catalytic conditions compared to uniform channel reactors and stronger mass transfer capabilities. The larger the proportion of internal channels, the more intense the effect. This study provides a new reactor preparation strategy for continuous fluid catalysis owing to the low cost and simple process; the proposed strategy is expected to create wide application prospects for continuous fluid catalysis in industrial flow catalytic reactions.

Author contributions

En-Jiang Liu: writing – original draft, investigation, formal analysis. Yu-shi Shen: writing – original draft, investigation, formal analysis. Mei-Yan Ling: formal analysis. Chen-Xi He: formal analysis. Xing Zhou: investigation. Jun Wang: supervision. Shuai You: validation. Wei-Guo Zhao: supervision. Xiao-Hui Yao: supervision. Dong-Yang Zhang: conceptualization, funding acquisition, project administration.

Conflicts of interest

We declare that we have no financial and personal relationships with other people or organizations that can inappropriately influence our work, there is no professional or other personal interest of any nature or kind in any product, service and/or company that could be construed as influencing the position presented in, or the review of, the manuscript entitled, “Wood-inspired dual-scale directional channels cellulose bioreactors with high mass transfer efficiency for continuous flow catalytic green conversion”.

Acknowledgements

This work was supported by Natural Science Foundation of Jiangsu Province (BK20231253), Six talent peaks project in Jiangsu Province (SWYY-155), Postdoctoral Research Fund project of Jiangsu Province (2021K253B), the earmarked fund

for CARS-18, National Key R&D Program of China, Key projects of international scientific and technological innovation co-operation (2021YFE0111100), Guangxi innovation-driven development project (AA19182012-2) and Zhenjiang Science and Technology support project (GJ2021015).

References

1 L. Buglioni, F. Raymenants, A. Slattery, S. D. Zondag and T. Noel, *Chem. Rev.*, 2022, **122**, 2752–2906.
2 Y. Zhu, Q. Chen, L. Shao and Y. Jia, *React. Chem. Eng.*, 2020, **5**, 9–32.
3 D. Yi, T. Bayer, C. P. S. Badenhorst, S. Wu, M. Doerr, M. Hohne and U. T. Bornscheuer, *Chem. Soc. Rev.*, 2021, **50**, 8003–8049.
4 P. D. Santis, L.-E. Meyer and S. Kara, *React. Chem. Eng.*, 2020, **5**, 2155–2184.
5 W. Tang, S. Zhu, D. Jiang, L. Zhu, J. Yang and N. Xiang, *Lab Chip*, 2020, **20**, 3485–3502.
6 A. Rogolino and G. Savio, *Mater. Adv.*, 2021, **2**, 845–855.
7 E. J. S. Brás, V. Chu, J. P. Conde and P. Fernandes, *React. Chem. Eng.*, 2021, **6**, 815–827.
8 N. Xiang and Z. Ni, *Lab Chip*, 2022, **22**, 4792–4804.
9 L. Wan, M. Jiang, D. Cheng, M. Liu and F. Chen, *React. Chem. Eng.*, 2022, **7**, 490–550.
10 A. Sivo, R. D. S. Galaverna, G. R. Gomes and J. C. Pastre, *React. Chem. Eng.*, 2021, **6**, 756–786.
11 A. Shakeri, S. Khan and T. F. Didar, *Lab Chip*, 2021, **21**, 3053–3075.
12 K. Tu, B. Puertolas, M. Adobes-Vidal, Y. Wang, J. Sun, J. Traber, I. Burgert, J. Perez-Ramirez and T. Keplinger, *Adv. Sci.*, 2020, **7**, 1902897.
13 F. Chen, A. S. Gong, M. Zhu, G. Chen, S. D. Lacey, F. Jiang and L. Hu, *ACS Nano*, 2017, **11**, 4275–4282.
14 J. Li, C. Chen, W. Gan, Z. Li and L. Hu, *J. Mater. Chem. A*, 2021, **9**, 9745–9752.
15 Y. S. Shen, X. Zhou, S. You, L. C. Gong, J. Wang, T. Chen, W. G. Zhao, X. H. Yao and D. Y. Zhang, *Green Chem.*, 2023, **25**, 1030–1039.
16 R. Z. Hu, X. Q. Zhang, X. H. Yao, J. X. Yang, E. J. Liu, T. Chen, Y. J. Fu, W. G. Zhao and D. Y. Zhang, *Ind. Crops Prod.*, 2022, **179**, 114690.
17 Y. S. Shen, X. H. Yao, C. X. He, R. Z. Hu, J. X. Yang, D. Y. Zhang and T. Chen, *Ind. Crops Prod.*, 2022, **178**, 114589.
18 C. X. He, Y. S. Shen, M. Y. Ling, X. H. Yao, T. Chen, W. G. Zhao and D. Y. Zhang, *Sustainable Chem. Pharm.*, 2023, **33**, 101082.
19 D. Y. Zhang, Y. Wan, X. H. Yao, C. Chen, Y. X. Ju, F. F. Shuang, Y. J. Fu, T. Chen, W. G. Zhao and L. Liu, *Ind. Crops Prod.*, 2020, **144**, 112029.
20 M. A. Shahbazi, M. Ghalkhani and H. Maleki, *Adv. Eng. Mater.*, 2020, **22**, 2000033.
21 G. Shao, D. A. H. Hanaor, X. Shen and A. Gurlo, *Adv. Mater.*, 2020, **32**, e1907176.
22 F. Zhao, L. Lin, J. Zhang, J. Liu, J. Shi, Y. L. Godec and A. Courac, *Adv. Mater. Technol.*, 2023, **8**, 2201968.
23 C. Gao, J. Yang, H. Zhang, W. Xiao and L. Han, *Bioresour. Technol.*, 2020, **312**, 123535.
24 R. Z. Hu, X. Q. Zhang, X. H. Yao, J. X. Yang, E. J. Liu, T. Chen, Y. J. Fu, W. G. Zhao and D. Y. Zhang, *Ind. Crops Prod.*, 2022, **179**, 114690.
25 M. K. Alavijeh, A. S. Meyer, S. L. Gras and S. E. Kentish, *ACS Sustainable Chem. Eng.*, 2020, **8**, 16205–16216.
26 I. Delfino, M. Portaccio, B. Della Ventura, D. G. Mita and M. Lepore, *Mater. Sci. Eng., C*, 2013, **33**, 304–310.
27 K. Rodriguez-Nunez, F. Lopez-Gallego, R. Martinez and C. Bernal, *Int. J. Biol. Macromol.*, 2023, **242**, 125075.
28 N. A. Daronch, M. Kelbert, C. S. Pereira, P. H. H. d. Araújo and D. d. Oliveira, *Chem Eng J.*, 2020, **397**, 125506.
29 J. Zdarta, K. Jankowska, K. Bachosz, E. Kijeńska-Gawrońska, A. Zgoła-Grześkowiak, E. Kaczorek and T. Jesionowski, *Catal. Today*, 2020, **348**, 127–136.
30 S. He, C. Chen, Y. Kuang, R. Mi, Y. Liu, Y. Pei, W. Kong, W. Gan, H. Xie and E. Hitz, *Energy Environ. Sci.*, 2019, **12**, 1558–1567.
31 S. He, C. Chen, G. Chen, F. Chen and L. Hu, *Chem. Mater.*, 2020, **32**, 1887–1895.
32 J. Ding, X. Wang, X. Zhou, N. Ren and W. Guo, *Bioresour. Technol.*, 2010, **101**, 7005–7013.
33 D. Davis, M. Troiano, A. Chinnici, W. Saw, T. Lau, R. Solimene and G. Nathan, *Chem. Eng. Sci.*, 2020, **214**, 115421.
34 B. Choi, B. Wan, S. Philyaw, K. Dhanasekharan and T. Ring, *Ind. Eng. Chem. Res.*, 2004, **43**, 6548–6556.
35 A. E. Rodrigues, *Chem. Eng. Sci.*, 2021, **230**, 116188.
36 X. Cui, M. Mannan and B. Wilhite, *Chem. Eng. Sci.*, 2015, **137**, 487–503.
37 H. Liu, J. Jiang and W. Zhai, *Chem. Eng. J.*, 2022, **449**, 137870.
38 V. Gowd, K. Kanika, C. Jori, A. Chaudhary, H. A. Rudayni, S. Rashid and R. Khan, *J. Nutr. Biochem.*, 2022, **109**, 109101.
39 R. Li, L. Liu, K. Dominic, T. Wang, T. Fan, F. Hu, Y. Wang, L. Zhang, L. Li and W. Zhao, *Plant Physiol. Biochem.*, 2018, **132**, 603–611.
40 M. Ackah, L. Guo, S. Li, X. Jin, C. Asakiya, E. Aboagye, F. Yuan, M. Wu, L. Essoh, D. Adjibolosoo, T. Attaribo, Q. Zhang, C. Lin and W. Zhao, *Plants*, 2022, **11**, 190.
41 R. Li, D. Chen, T. Wang, Y. Wan, R. Li, R. Fang, Y. Wang, F. Hu, H. Zhou, L. Li and W. Zhao, *PLoS One*, 2017, **12**, e0172883.
42 J. Zhou, S. Li, W. Wang, X. Guo, Xi. Lu, X. Yan, D. Huang, B. Wei and L. Cao, *Sci. World J.*, 2013, **2013**, 380692.
43 Z. Li, X. Chen, G. Liu, J. Li, J. Zhang, Y. Cao and J. Miao, *Molecules*, 2021, **26**, 7574.
44 Q. Liu, Y. Qin, B. Jiang, J. Chen and T. Zhang, *Col. Surf. B*, 2022, **216**, 112529.
45 S. Bo, S. K. Chang, T. Zhou, H. Zhu, Y. Jiang and B. Yang, *Food Chem.*, 2022, **378**, 132118.

46 X. H. Fan, L. T. Wang, J. Y. An, S. D. Zhang, Z. H. Cai, L. L. Niu, P. Kou, Q. Yang, D. Meng and Y. J. Fu, *Ind. Crops Prod.*, 2021, **161**, 113213.
47 S. Jin, M. Luo, W. Wang, C. J. Zhao, C. B. Gu, C. Y. Li, Y. G. Zu, Y. J. Fu and Y. Guan, *Bioresour. Technol.*, 2013, **136**, 766–770.
48 D. Y. Zhang, Y. Wan, X. H. Yao, C. Chen, Y. X. Ju, F. F. Shuang, Y. J. Fu, T. Chen, W. G. Zhao and L. Liu, *Ind. Crops Prod.*, 2020, **144**, 112029.
49 X. Song, L. Cui, J. Li, H. Yan, L. Li, L. Wen, Y. Geng and D. Wang, *LWT*, 2019, **103**, 192–198.
50 A. Maleki, H. Movahed, P. Ravaghi and T. Kari, *RSC Adv.*, 2016, **6**, 98777.
51 Z. Hajizadeh, K. Valadi, R. Taheri-Ledari and A. Maleki, *ChemistrySelect.*, 2020, **5**, 2441–2448.
52 R. Eivazzadeh-Keihan, F. Khalili, N. Khosropour, H. A. M. Aliabadi, F. Radinekiyan, S. Sukhtezari, A. Maleki, H. Madanchi, M. R. Hamblin, M. Mahdavi, S. Mohammad, A. Haramshahi, A. E. Shalan and S. Lanceros-Mendez, *ACS Appl. Mater. Interfaces*, 2021, **13**, 33840–33849.
53 R. Eivazzadeh-Keihan, F. Radinekiyan, H. Madanchi, H. A. M. Aliabadi and A. Maleki, *Carbohydr. Polym.*, 2020, **248**, 116802.